Electronic Supplementary Information

Decoding lithium's subtle phase stability with a machine learning force field

Yiheng Shen[a] and Wei Xie*[a]

[a] Materials Genome Institute, Shanghai University, Shanghai 200444, China.

*Corresponding Author: xiewei@xielab.org

Note S1. MACE force field training

The training set for the MACE force field is generated as follows. Supercells of *bcc*-, *fcc*- and 9R-Li are generated from their pristine and strained primitive cells. The strain values, supercell matrices and temperature values used in the generation of phonon-rattled structrues are summarized in Table S1. For each strained primitive cell, five phonon-rattled supercells are respectively generated at 300, 600 and 900 K, yielding a total of 15 structures per primitive cell and thus a total of 15 structures per strain value × 5 strain values per system × 3 systems = 225 structures.

Table S1 Strain values and the supercell matrices for generating rattled structrues of *bcc*-, *fcc*- and 9R-Li, together with the number of atoms in respective primitve cell and supercell (N_{prim} and N_{sc}).

System	Strain values	Supercell matrix	N_{prim}	N_{sc}
bcc-Li	−0.03, −0.02, 0.0, 0.02, 0.05	$\begin{bmatrix} 0 & 6 & 6 \\ 6 & 0 & 6 \\ 6 & 6 & 0 \end{bmatrix}$	1	432
fcc-Li	−0.03, −0.02, 0.0, 0.02, 0.05	$\begin{bmatrix} -5 & 5 & 5 \\ 5 & -5 & 5 \\ 5 & 5 & -5 \end{bmatrix}$	1	500
9R-Li	−0.03, −0.02, 0.0, 0.02, 0.03	$\begin{bmatrix} -7 & 7 & 0 \\ 4 & 4 & -8 \\ -1 & -1 & -1 \end{bmatrix}$	3	504

First-principles calculations are performed on the rattled structures by using the Vienna *ab initio* simulations package (VASP)[1, 2] based on density functional theory, where the projector augmented wave method[3] is used for describing the interaction between valence electrons and ion cores, and the plane waves with an energy cutoff of

500 eV are used to expand the electron wave functions. The exchange-correlation interaction among the valence electrons is calculated by the PBE functional.[4, 5] The integration over the first Brillouin zone is performed on a 2×2×2 **k**-point grid in the Monkhorst−Pack scheme for calculating energy and interatomic forces in the supercell and a generalized regular **k**-point grid[6, 7] with KSPACING = 0.025 $Å^{-1}$ for calculating electronic entropy and enthalpy in the primitive cell. The convergence thresholds for the total energy during the self-consistent field iteration and the interatomic forces during the geometry optimization are set to 10^{-5} eV and 10^{-3} eV $Å^{-1}$, respectively.

As shown in Fig. S1a and S1b, KSPACING = 0.025 $Å^{-1}$ and energy cutoff of 500 eV yielded converged energy profile, with denser **k**-point grid (smaller KSPACING value) and higher energy cutoff amending the energy by less than 0.1 meV/atom. The 2×2×2 **k**-point grid for the pristine and strained supercells of *bcc*-, *fcc*- and 9R-Li in our training data aligns with the converged grid density of 0.025. The phase-resolved lattice parameters optimized with different exchange correlation functionals are comparable (Fig. S1c). The converged lattice parameters and energy profiles are summarized in Table S1, which consists with previous studies, e.g., the energy of *fcc*-Li is lower than that of *bcc*-Li by 2 meV/atom.[8]

The MACE force field quantitatively reproduced the energy difference between *bcc*- and *fcc*-Li, as summarized in Table S1, which is not a trivial task since it approaches the RMSE of the force field. In addition, the MACE force field reproduces the energy profile of *bcc*-, *fcc*- and 9R-Li upon compression to atomic volume of about 13 $Å^3$, as shown in Fig. S2, validating its application in high-pressure simulations.

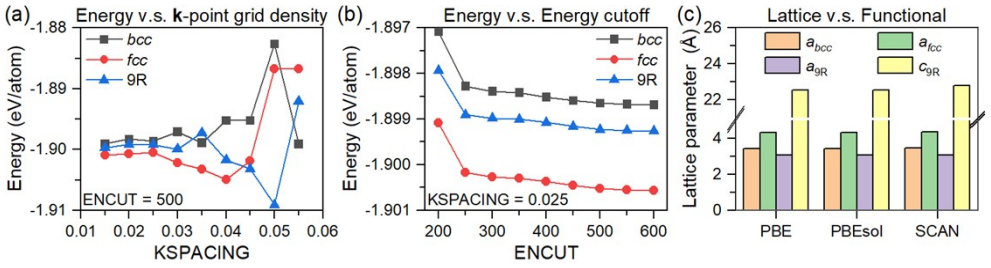

Fig. S1 Energy over (a) KSPACING parameter for generalized regular **k**-point grid density and (b) energy cutoff. (c) Lattice parameters optimized with different exchange-correlation functionals.

Table S1 Phase resolved equilibrium lattice parameters a_{fcc}, a_{bcc}, a_{9R}, c_{9R} (in Å) and energy difference ΔE between *bcc*- and *fcc*-Li (in meV/atom) predicted by DFT and MLIPs in this work and previous researches. Energy cutoff (E_{cut}, in eV) and k-point grid density (d, in Å^{-1}) for DFT simulations are provided for reference.

Model	a_{fcc}	a_{bcc}	a_{9R}	c_{9R}	ΔE	E_{cut}	d
DFT (this work)	4.330	3.440	3.061	22.52	1.9	500	0.025
MACE (this work)	4.338	3.436	3.101	22.76	2.2	--	--
DFT[8]	--	3.427	--	--	2	1360	0.02
DeepMD[8]	--	3.434	--	--	1	--	--
NequIP64[8]	--	3.429	--	--	1	--	--

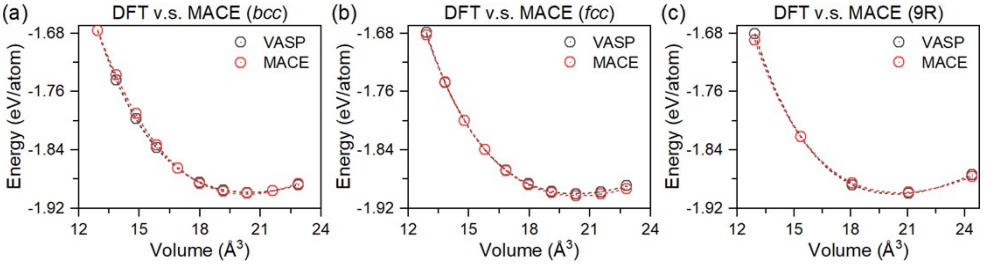

Fig. S2 Energy of (a) *bcc*-, (b) *fcc*- and (c) 9R-Li upon isotropic change of volume, as calculated by VASP (black) and MACE force field (red).

Note S2. SCP and thermodynamic calculations

In each SCP iteration, 100 rattled supercells, whose supercell matrices are identical with those during the generation of training data for the MACE force field, are generated from the latest effective harmonic model $\mathbf{\Phi}_{n-1}$ *via* phonon rattling. The interatomic forces of these rattled supercells are then calculated by the MACE force field. The new effective harmonic model $\mathbf{\Phi}_n$ is obtained from a linear mixing of the least-square fit of the force-displacement relation in the rattled supercells and $\mathbf{\Phi}_{n-1}$ with mixing parameter alpha = 0.1. A total of 30 SCP iterations are performed at each temperature studied. That is, interatomic forces in 30 × 100 = 3000 rattled supercells were calculated to obtain SCP in a given lattice at a single temperature. Evaluating the interatomic forces of a 500-atom supercell of *fcc*-Li required approximately one hour using 64 CPU cores with DFT-VASP, and less than one second using a single NVIDIA V100 GPU with MACE. This represents a three-orders-of-magnitude speedup in wall-clock time, even before considering that buying 64 CPU hours is typically more expensive than one V100 GPU hour from most high-performance computing service providers. A complete self-consistent phonon (SCP) calculation cycle necessitates the evaluation of approximately two million such supercells. This translates to an estimated 500 GPU hours using MACE, compared to approximately 100 million CPU hours using VASP, a cost that is likely prohibitive and perhaps unprecedented.

Vibrational Helmholtz free energy F_{vib} is calculated from the effective harmonic frequencies $\omega_{\mathbf{q}\nu}$ obtained from SCP by

$$F_{\mathrm{vib}} = U_0 + \frac{1}{2}\sum_{\mathbf{q}\nu} \mathsf{h}\omega_{\mathbf{q}\nu} + k_{\mathrm{B}}T\sum_{\mathbf{q}\nu} \ln\left[1 - \exp\left(-\frac{\mathsf{h}\omega_{\mathbf{q}\nu}}{k_{\mathrm{B}}T}\right)\right],$$

where **q** is the reciprocal coordinate, *v* is the phonon band index, and

$$U_0 = \left\langle V\left(\mathbf{R}_0 + \mathbf{x}\right) - \frac{1}{2}\mathbf{x}^{\mathrm{T}}\boldsymbol{\Phi}_{\mathrm{eff}}^{(2)}(T)\mathbf{x} \right\rangle$$

is the reference energy, $V(\mathbf{R})$ is the potential energy surface represented by the MACE force field, $\boldsymbol{\Phi}_{\mathrm{eff}}^{(2)}$ is the effective harmonic model from SCP calculation, **x** is the displacement with respective to the equilibrium configuration $\mathbf{R}_0$, and <·> denotes the ensemble average over the phonon rattling **x** with Bose−Einstein distribution. The summation over **q** is performed on uniformed grids of 26×26×26 for *bcc*-Li, 16×16×16 for *fcc*-Li and 18×18×18 for 9R-Li, so that the their free energy values are respectively converged to < 0.1 meV/atom.

Note S3. Free energy fitting

The fitting of the Helmholtz free energy F as a function of lattice parameter(s) **A** is not a trivial task. When raw SCP data are calculated at uneven portions of compressive and tensile strained lattice parameters, ordinary least-squares (OLS) fitting provides poor results, as it is sensitive to the number of high-energy raw data points. Take the Helmholtz free energy of *bcc*-Li at T = 350 K and 0 GPa as an example, when we successively discard the most compressed raw data point, the fitted curves change dramatically around their minima (Fig. S3b) despite the visual similarity in the entire range (Fig. S3a) and the high R^2 values of over 0.999.

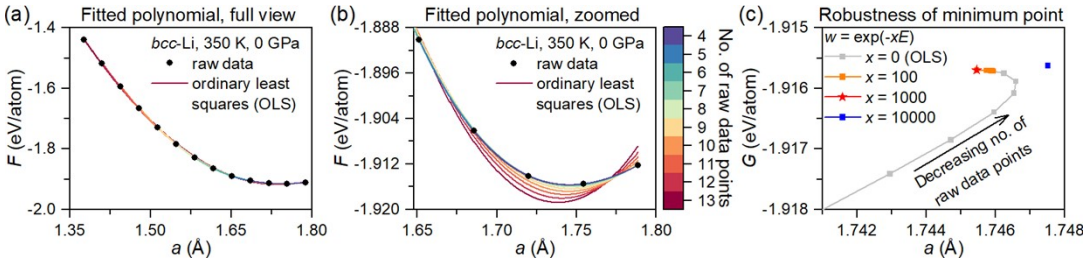

Fig. S3 Helmholtz free energy F of bcc-Li as a function of lattice parameter a at 350 K and 0 GPa: (a) full view of all 13 raw data points (black dots) from SCP calculations and the fitted curves, and (b) zoomed-in view near the equilibrium lattice and the fitted curves, showing only five visible raw data points. Color of the curves differentiates the number of raw data points fitted to (see the color palate on the right). (c) Evolution of minimum points from 3rd-order polynomials fitted with different weight functions.

To obtain robust fitting results, we performed weight least squares (WLS) fitting instead. That is, the raw data is considered with weight $w(E) = \exp(-xE)$ in the least squares fitting, where x is an empirical parameter and E (in eV/atom) is the sum of Helmholtz free energy F and the volumetric term pV, i.e. $E = F + pV$. Proper x value was explored and set respectively to 1000, 1000 and 300 for *bcc*-, *fcc*- and 9R-Li, where

smaller values cannot cancel out the data dependency and larger values tend to overly bias the minimum of the fitted curve toward the minimal raw data. For comparison, we compared the results from OLS (left) and WLS (right) fitting in Fig. S4 and S5. One can see that the errors from OLS fitting result in qualitatively wrong prediction of 9R-Li as ground.

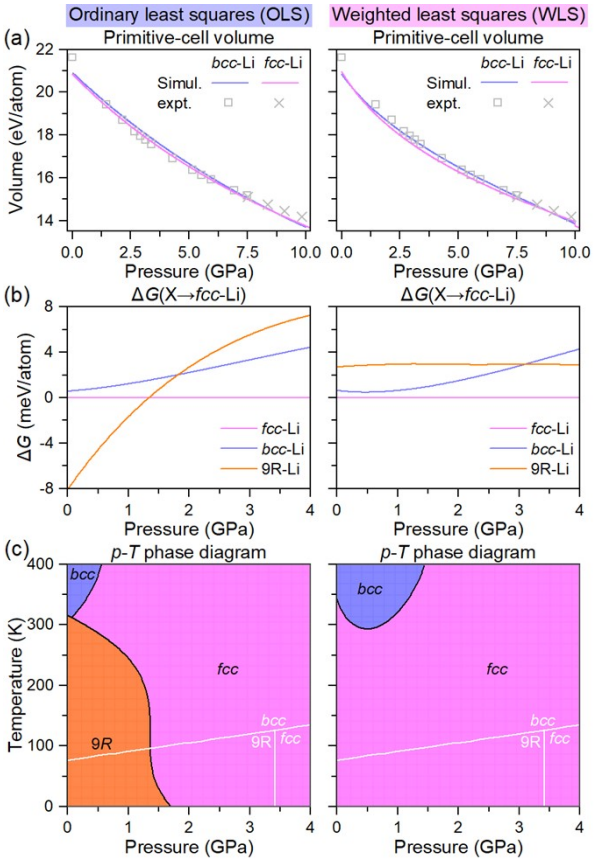

Fig. S4 Pressure-dependent (a) primitive unit cell volume (at 300 K), (b) Gibbs free energy difference (at 200 K) and (c) phase diagram as predicted from ordinary least squares (OLS) (left) and weighted least squares (WLS) (right) fittings, respectively using raw SCP data.

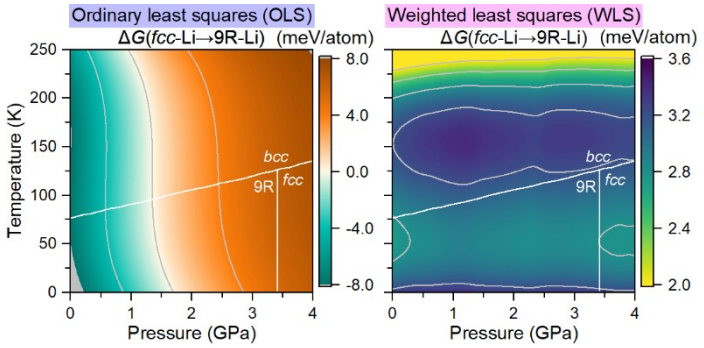

Fig. S5 Gibbs free energy difference between *fcc*- and 9R-Li calculated from ordinary least squares (OLS) (left) and weighted least squares (WLS) (right) fittings, respectively.

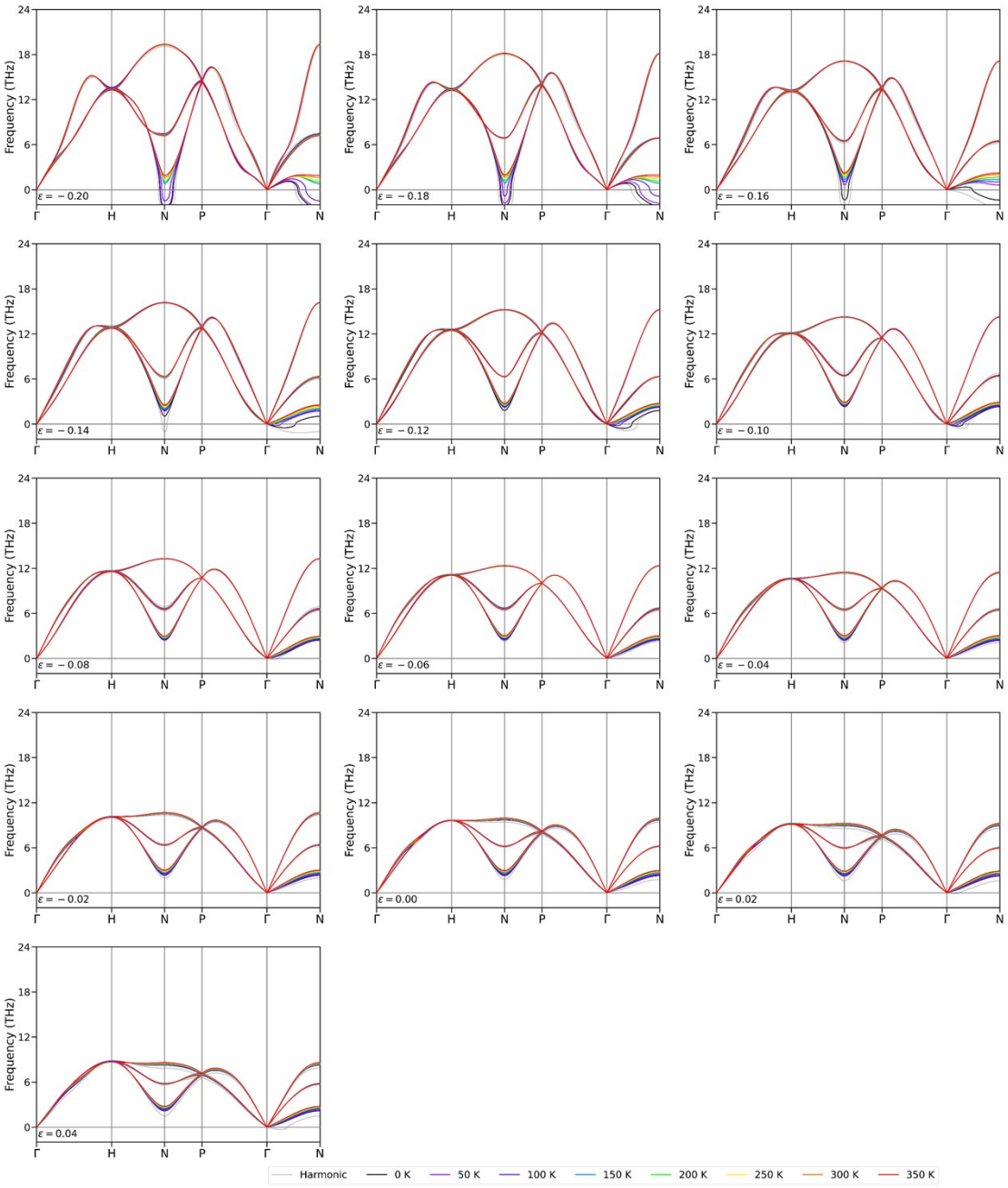

Fig. S6 Phonon band structures of *bcc*-Li under equiaxial strain ε.

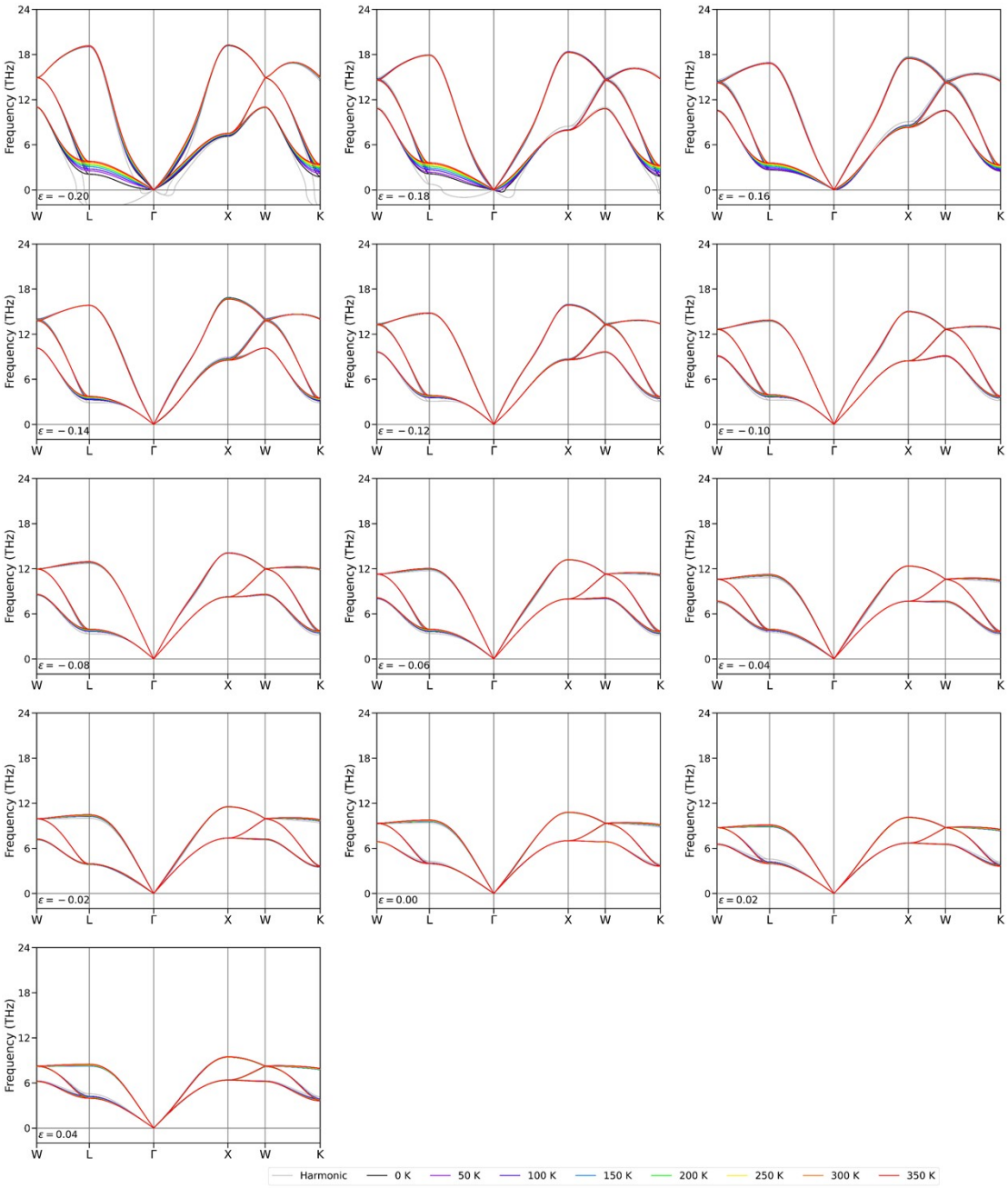

Fig. S7 Phonon band structures of *fcc*-Li under equiaxial strain ε.

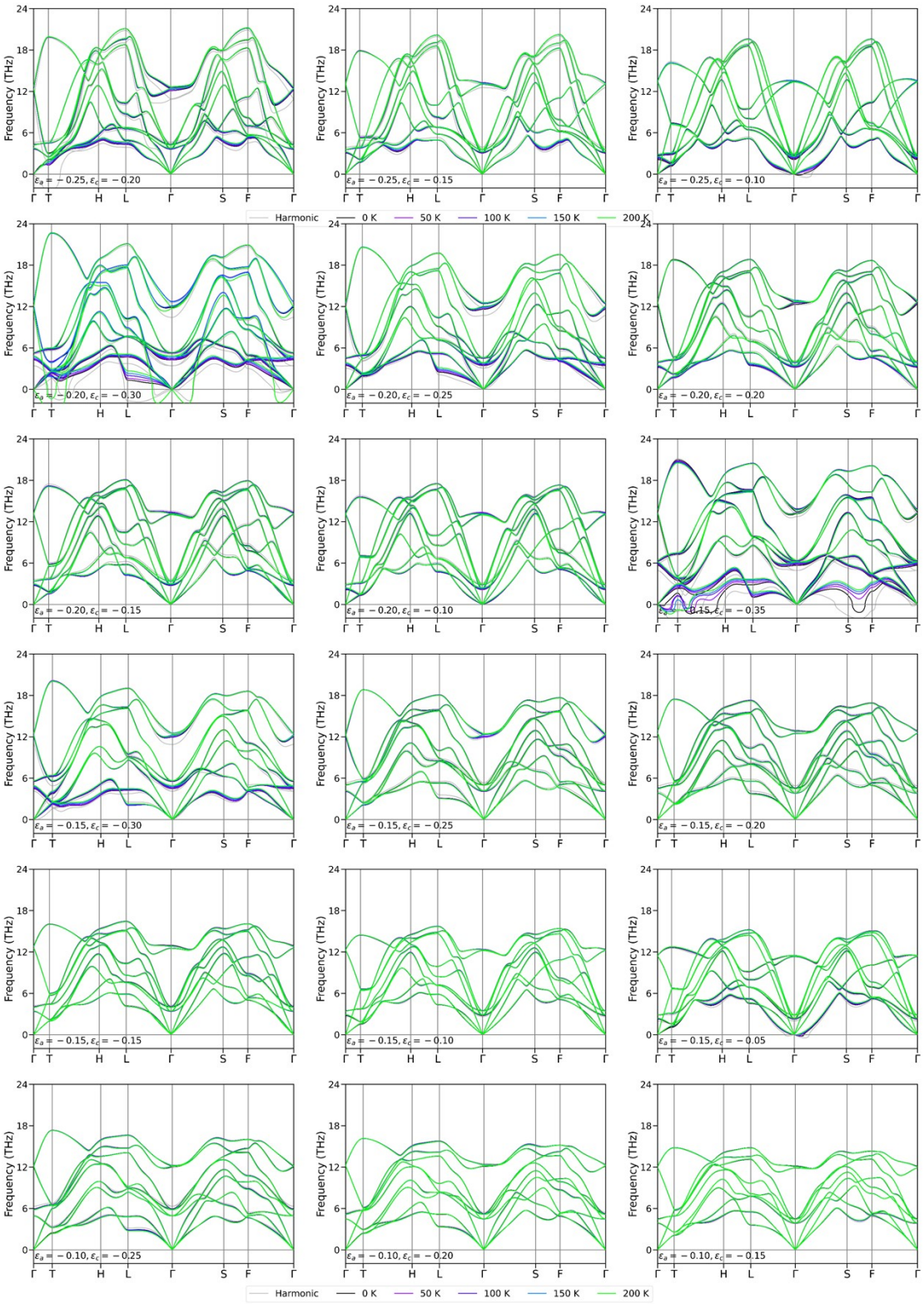

Fig. S8 Phonon band structures of 9R-Li under biaxial strain ε_a and uniaxial strain ε_c.

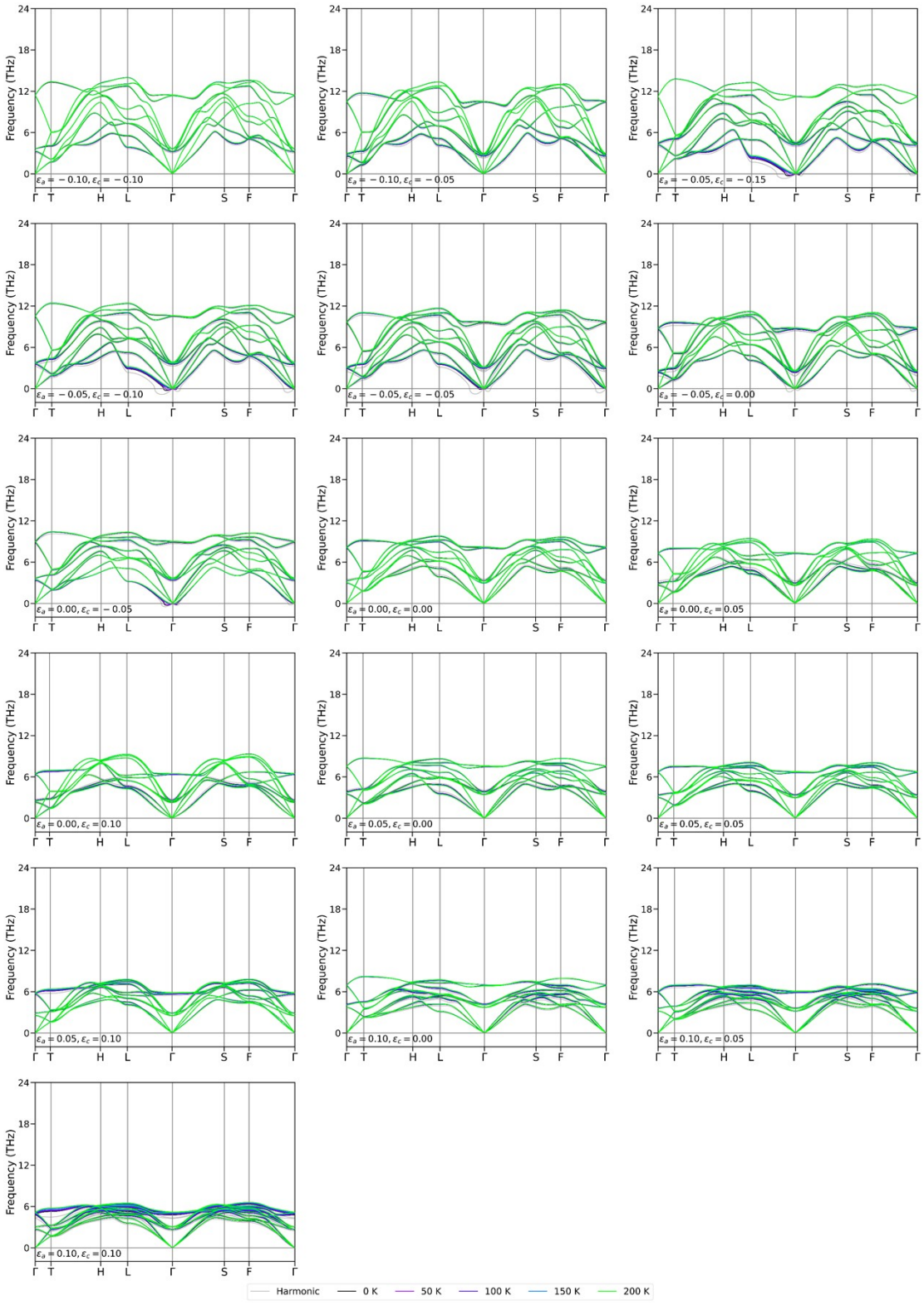

Fig. S8 (continued) Phonon band structures of 9R-Li under biaxial strain ε_a and uniaxial strain ε_c.

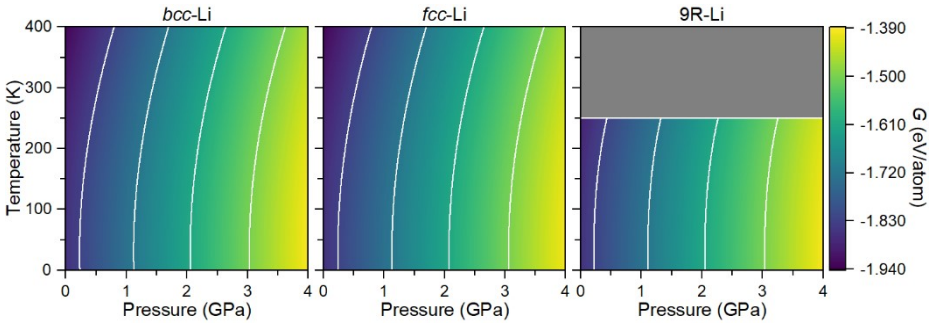

Fig. S9 Temperature- and pressure-dependent equilibrium Gibbs free energy of *bcc*-, *fcc*- and 9R-Li. Grey region in 9R-Li panel represents missing data to avoid over-extrapolation from calculated results.

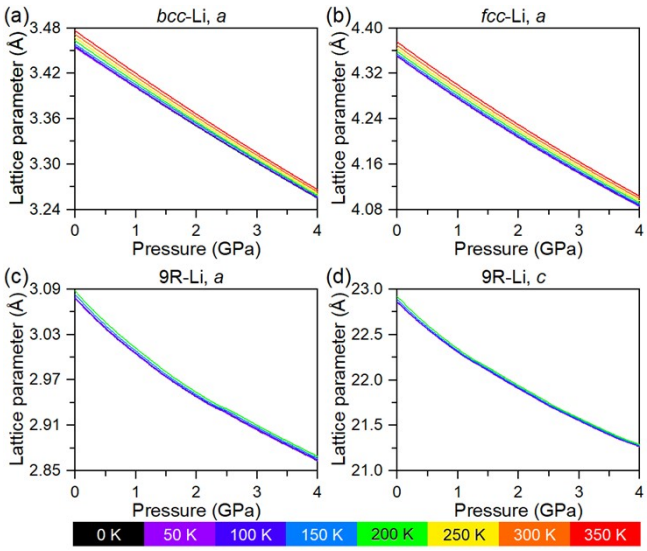

Fig. S10 Temperature- and pressure-dependent equilibrium lattice parameters of (a) *bcc*-Li, (b) *fcc*-Li and (c-d) 9R-Li. Analogous results calculated at QHA level using the MACE force field is shown in Fig. S13.

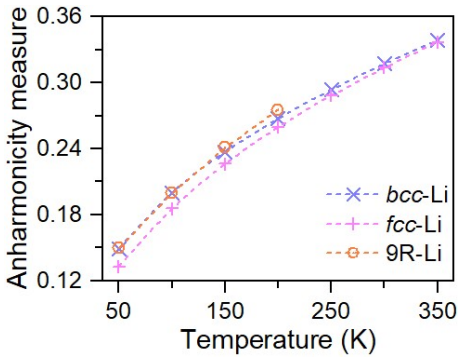

Fig. S11 Analogous of Fig. 3, but excluding nuclear quantum effects.

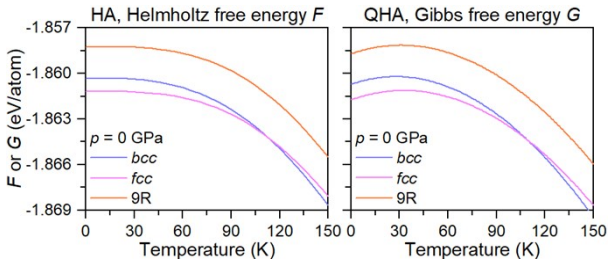

Fig. S12 Free energy profile of *bcc*-, *fcc*- and 9R-Li calculated at HA and QHA level, with respective predicted phase-equilibrium temperature of 112 and 109 K.

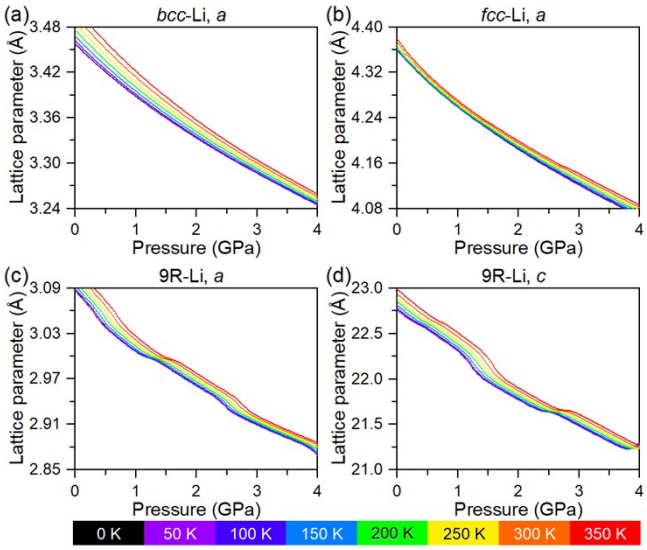

Fig. S13 Analogous of Fig. S10, but calculated at QHA level using the MACE force field. Anomaly in equilibrium lattice parameters of 9R-Li around 2 GPa could indicate overfitted double-well polynomial from errored flat free energy profile around that section. In general, thermal expansion is more extensive as compared to results in Fig. S10.

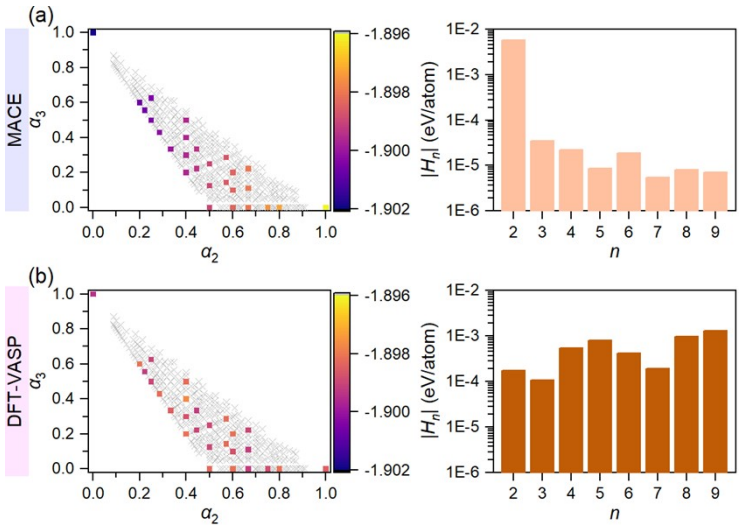

Fig. S14 (a) Realizable close-packed stacking variants up to 22 layers per repeating unit, projected on the α_2-α_3 plane. Configurations of up to 10-layer stacking were optimized by the MACE force field and colored according to its energy. (b) Absolute value of fitted H_n parameters in logarithmic coordinate.

References

1. G. Kresse and J. Furthmuller, *Phys. Rev. B*, 1996, **54**, 11169-11186.
2. G. Kresse and J. Furthmuller, *Comput. Mater. Sci.*, 1996, **6**, 15-50.
3. P. E. Blöchl, *Phys. Rev. B*, 1994, **50**, 17953-17979.
4. J. P. Perdew, K. Burke and M. Ernzerhof, *Phys. Rev. Lett.*, 1996, **77**, 3865-3868.
5. J. P. Perdew, M. Ernzerhof and K. Burke, *J. Chem. Phys.*, 1996, **105**, 9982-9985.
6. W. S. Morgan, J. J. Jorgensen, B. C. Hess and G. L. W. Hart, *Comput. Mater. Sci.*, 2018, **153**, 424-430.
7. G. L. W. Hart, J. J. Jorgensen, W. S. Morgan and R. W. Forcade, *J. Phys. Commun.*, 2019, **3**, 065009.
8. M. K. Phuthi, A. M. Yao, S. Batzner, A. Musaelian, P. Guan, B. Kozinsky, E. D. Cubuk and V. Viswanathan, *ACS Omega*, 2024, **9**, 10904-10912.